New lens system for surface vibrational spectroscopy at high impact energies

R. L. Strong and J. L. Erskine

Department of Physics, University of Texas, Austin, Texas 78712

(Received 15 March 1984; accepted for publication 25 April 1984)

The design, characterization, and performance of a new lens system which permits high-resolution electron energy-loss spectroscopy (EELS) studies at high energies is described. The lens system can be adapted to most existing EELS instruments and extends the impact energy range to 300 eV. Electron ray-tracing techniques are used to characterize operating modes of one of the more common EELS optics designs as well as the new lens configuration. The results presented in this paper demonstrate some limitations of matrix optics approaches and the applicability of electron ray-tracing techniques for characterizing the transmission properties, angular profiles, image sizes, and operating modes of EELS spectrometers.

INTRODUCTION

High-resolution electron energy-loss spectroscopy (EELS) is rapidly becoming one of the most useful techniques for probing physical and chemical phenomena at surfaces. The EELS technique is based on detection of quantum energy losses in a monoenergetic electron beam scattered from a surface. Quantum energy losses (or gains) at surfaces result from excitations involving intrinsic surface vibrations (surface phonons) or vibrations of adsorbed atomic or molecular species. The technique combines high surface sensitivity (0.001 monolayer coverages can be detected in ideal cases) with a broad spectral range (good spectrometers are able to measure losses below 20 meV). In addition, EELS is one of the few surface sensitive techniques which can be considered a molecular spectroscopy rather than an atomic one.

The importance of studying vibrational properties of matter has been recognized for many years. Vibrational spectra provide information which is closely related to microscopic forces in matter and, in many cases, simple models and symmetry relations, in conjunction with vibrational data, can lead directly to important insight into the structure. This direct relationship between experimental data and molecular level physical parameters is one feature which seems to characterize the most useful spectroscopic probes.

Recent experimental results which combine EELS data with lattice dynamical calculations have emphasized the potential of using vibrational spectroscopy to investigate surface crystallography. EELS studies of the O/Al (111) system combined with lattice dynamical calculations have shown that surface complexes consisting of both overlayer and underlayer chemisorbed species can be investigated.[1] Similar investigations of the O/Ni (100) system have shown that EELS data combined with lattice dynamical models can be used to test structural models and adsorbate bond distances.[2,3] The dispersion of intrinsic surface phonon bands on Ni (100) has been recently measured using EELS.[4] Intrinsic phonon band mapping and detection of adsorbate vibrational modes having eigenvectors parallel to the surface generally require a nonspecular scattering configuration (refer to Fig. 1). In nonspecular scattering geometry, vibrational losses result from the impact scattering mechanism,[5,6] whereas vibrational losses observed using specular geometry are generally due to dipole scattering.[7]

The incident energy dependence of dipole scattering and impact scattering is different and, as will be discussed in the next section, the two scattering mechanisms differ in several other important aspects. In general, it is preferable to study dipole scattering vibrational losses at lower impact energies and impact scattering vibrational losses at higher impact energies. Most existing EELS spectrometers have been designed to study dipole vibrational losses. Therefore, the lens systems and control electronics typically permit electron scattering studies at energies up to 20 eV, but not at energies of several hundred electron volts which are often required for some impact scattering experiments.

This paper describes a straightforward lens system modification of one of the more common EELS spectrometer designs which permits operation of the spectrometer at impact energies above 300 eV. Electron ray-tracing techniques are used in the new lens design, and are also used to

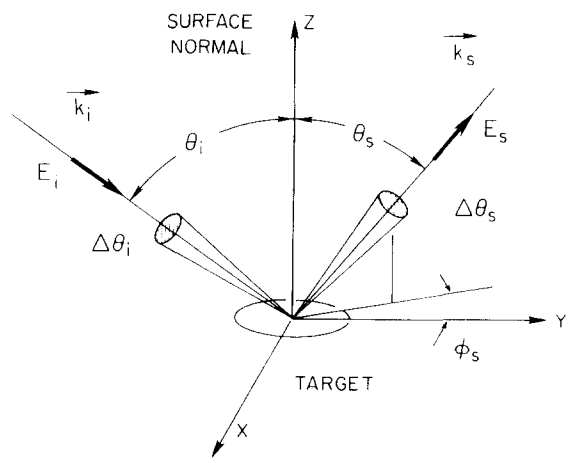

FIG. 1. Scattering geometry and parameters. Specular geometry $\theta_i = \theta_s$ and $\phi_s = 0$; off-specular geometry, $\theta_i \neq \theta_s$ or $\phi_s \neq 0$. E_i and E_s refer to incident and scattered electron energy. $\mathbf{k}_i$ and $\mathbf{k}_s$ are the electron incident and scattered wave vectors.

 0034-6748/84/081304-06$01.30

determine the beam profiles and image characteristics associated with spectrometer operating modes established empirically. (An operating mode consists of the set of lens voltages established by maximizing the counting rate for a given beam energy.) These studies have shown that ray-tracing is a valuable tool for understanding and optimizing the performance of high-resolution electron scattering optics.

I. ELECTRON SCATTERING MECHANISMS

To better understand the motivation for extending the scattering energy range of EELS spectrometers, it is helpful to briefly consider what has been established about electron scattering phenomena at surfaces. It is now well established that two distinct scattering regimes are required to account for experimental observations of vibrational losses measured by inelastic electron scattering from surfaces. The basic difference between these two regimes is that one is based on long-range dipolar fields which produce small-angle (forward) inelastic scattering,[7] and the other is based on short-range atomic-like fields which produce large-angle (diffuse) inelastic scattering.[5]

Vibrational losses observed using specular geometry (refer to Fig. 1) generally result from the "dipole" scattering mechanism.[7] In this scattering regime, the process is viewed as a combination of inelastic forward scattering by dipolar fields followed or preceded by elastic backscattering (reflection) from the surface. Dipole scattering is, therefore, characterized by a narrow angular spread around the specular scattering angle. A careful analysis of dipole scattering shows that due to the finite energy loss, two lobes appear on either side of the specular angle having an angular separation $\Delta\theta_s = \pm \Delta E/2E_i$, where ΔE is the energy loss and E_i is the incident energy. In addition, the dipole cross section integrated over these two forward scattering lobes is proportional to $E_i^{-3/2}$. This implies that one characteristic of dipole scattering is a ratio of loss peak intensity to elastic peak intensity which varies as $E_i^{-3/2}$, if the reflectivity of the crystal is a slowly varying function of energy.

A second and distinctly different scattering regime termed "impact" scattering is associated with short-ranged atomic-like potentials.[5] Electrons scattered by vibrational excitations in this regime exhibit a more isotropic angular spread.[6] In addition, the cross-section energy dependence is no longer a simple monotonic function of E_i and in fact contains structure which is related to bond distances and other surface crystallographic parameters.[5,8] The most striking difference between these two scattering mechanisms, from an experimental point of view, is the relative magnitude of the differential scattering cross sections. The total scattering cross section for impact scattering is comparable to (or larger than) dipole cross sections. However, under typical experimental conditions, when the energy analyzer defines a small acceptance cone (typically $\Delta\theta_s$ is 1° or less), the actual counting rate associated with the two scattering mechanisms is vastly different. For example, with a clean well-ordered crystal, state-of-the-art EELS spectrometers operating at 5-meV resolution yield elastic peak counting rates in specular geometry of about 10^5 Hz. A dipole loss feature measured using monolayer coverages will yield typical counting rates,

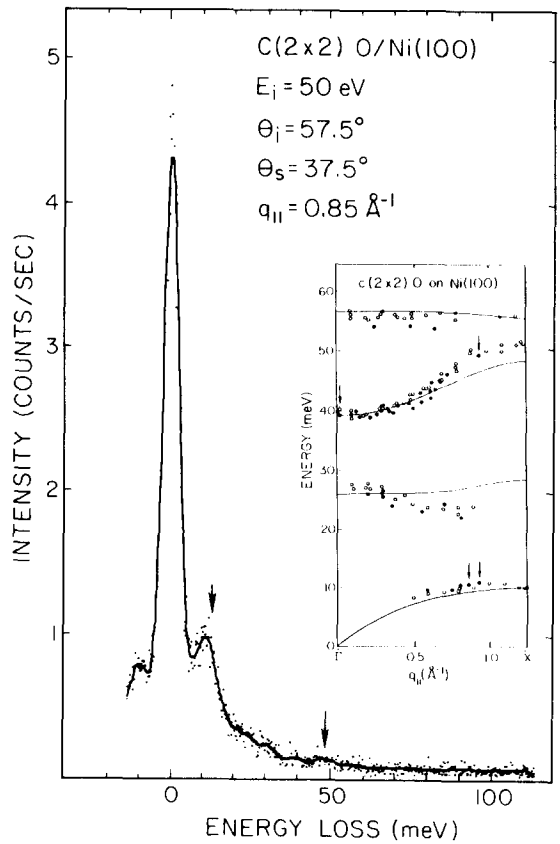

FIG. 2. EELS spectra for $c(2\times2)$O/Ni (100) taken in off-specular geometry at 50-eV impact energy. Inset illustrates calculated surface phonon bands along the $\bar{\Delta}$ line (Ref. 2). Open circles, data from Ref. 3, solid circles from Ref. 2. Points in inset indicated by arrows correspond to data for spectra illustrated in this paper.

under the same conditions, of a few hundred Hz, and an impact loss peak, observed under corresponding conditions, will yield a counting rate of the order of 1 Hz or less.

Energy and momentum conservation associated with the excitation of a phonon having energy $\hbar\omega$ require

$$E_i = E_s + \hbar\omega, \tag{1}$$

$$\mathbf{k}_i \sin\theta_i = \mathbf{k}_s \sin\theta_s + \mathbf{q}_{||} + \mathbf{G}, \tag{2}$$

where $\mathbf{G}$ is a two-dimensional reciprocal lattice vector (usually $\mathbf{0}$) and $\mathbf{q}_{||}$ is restricted to the first surface Brillouin zone. If θ_i and θ_s are the incidence and scattering angles measured from the surface normal, $|\mathbf{q}_{||}|$ is given by

$$|\mathbf{q}_{||}| = \frac{2m_e}{\hbar}|\sqrt{E_i}\sin\theta_i - \sqrt{E_i - \hbar\omega}\sin\theta_s| \tag{3}$$

or, if $\hbar\omega \ll E_i$,

$$|\mathbf{q}_{||}| = 0.512\sqrt{E_i(\text{eV})}\,|\sin\theta_i - \sin\theta_s|\,\text{Å}^{-1}. \tag{4}$$

From these equations, it is clear that independent of factors related to scattering cross sections, fairly high scattering energies are desirable to probe vibrational properties of the full surface Brillouin zone of a crystal surface. For example, the zone edge ($\bar{M}$ point) along the (11) direction ($\bar{\Sigma}$ line) of Ni (100) corresponds to $|\mathbf{q}_{||}| = 1.785$ Å^{-1}. Choosing $\theta_s = 40°$ and $\theta_i = 60°$ as typical scattering angles, one finds that E_i must be about 240 eV to probe phonon modes at the zone edge. Mapping dispersion curves also requires a well-

defined analyzer acceptance angle to achieve a well-defined value of $|\mathbf{q}_{\parallel}|$. From Eq. (4), one obtains, for $\theta_i \neq \theta_s$,

$$|\Delta \mathbf{q}_{\parallel}| = |\mathbf{q}_{\parallel}| \left(\frac{\Delta E_i}{2E_i} + \frac{\Delta\theta_i \cos\theta_i + \Delta\theta_s \cos\theta_s}{|\sin\theta_i - \sin\theta_s|} \right). \quad (5)$$

Thus, it is apparent that higher impact energies help maintain accurate control over $\Delta q_{\parallel}$. It turns out that smaller values of $\Delta\theta_i$ and $\Delta\theta_s$ are more conveniently achieved at higher energies because of fundamental constraints associated with electron trajectories in nondispersive electron optical systems. These considerations help rationalize the need for increasing the energy of EELS spectrometers.

Figure 2 illustrates the use of the conservation laws to obtain one point of the S_4 surface phonon dispersion curve for $c(2\times2)$O/Ni (100) along the $\bar{\Gamma}$–$\bar{X}$ direction. The loss spectra was taken at 50-eV impact energy and using 20° off-specular scattering geometry. The parameters correspond to $|\mathbf{q}_{\parallel}| = 0.85$ Å^{-1}. These scattering parameters yield a strong elastic peak signal and pronounced gain and loss peaks 11 meV either side of the elastic peak corresponding to excitations involving the S_4 surface phonon of $c(2\times2)$O/Ni (100). The energy loss from the EELS data is plotted (with other data) on the inset which shows the calculated E vs $\mathbf{q}_{\parallel}$ dispersion of the S_4 and other oxygen-derived surface phonons for $c(2\times2)$O on Ni (100).[2] The spectra in Fig. 2 also exhibits evidence for additional modes of the $c(2\times2)$O/Ni (100) surface as indicated by an arrow on the spectrum and on the calculated phonon bands. These modes are more apparent at other impact energies.

II. ELECTRON OPTICS

Figure 3 illustrates the basic features of a typical EELS spectrometer which consists of an electron source and monochromator, acceleration and deceleration lenses, an energy analyzer, and a detector. Many variations are possible in implementing a working instrument; designs have been reported based on spherical (SDA-180°),[10] cylindrical (CDA-127°),[11] and cylindrical mirror (CMA-42°)[12] dispersive elements. The CMA-42° geometry is more cumbersome than the other two configurations for angle-dependent measurements and, in this paper, only the other two configurations, which are compatible with the illustration in Fig. 3, are considered. The discussion in the present paper centers on the lens systems in relation to the range of impact energies accessible and the angular considerations related to Eq. (5). Other technical considerations for both spherical (SDA-180°) and cylindrical (CDA-127°) EELS instruments, such as factors relating to resolution and counting rates, have been considered previously.[13]

The impact energy of electrons hitting the target is basically the monochromator pass energy plus the voltage difference between the exit slit and the target. The energy loss of analyzed electrons is basically the voltage difference between the monochromator and analyzer slits, assuming each analyzer is operating at the same pass energy. The input and output lenses do not affect the impact energy or the energy of analyzed electrons; however, they perform a critical function: they control the imaging properties of the spectrometer. Without suitable lens systems the intensity of detected signals would be too weak for useful spectroscopic work.

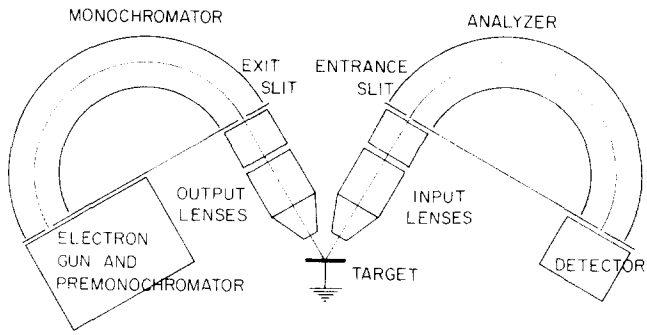

FIG. 3. Typical EELS spectrometer.

In arriving at a suitable lens system for a particular application, one of the most important considerations is the maximum acceleration and deceleration ratios which must be achieved. EELS measurements require energy resolution of the order of 5 meV. Various constraints related to magnetic shielding, size of the vacuum chamber, etc., have been considered in arriving at the physical dimensions and pass energies used in existing EELS optics. Typical instruments employ mean radii of a few centimeters, slit widths of a few tenths of a millimeter, and pass energies in the range of 0.2–2 eV. Instruments which are used primarily to study dipole losses are designed for impact energies in the 1–20 eV range. Higher energies are not necessary because dipole cross sections decrease with increasing energy. Impact energies of tens of electronvolts and pass energies of a few electronvolts or less require deceleration ratios of only a factor of 10. A single lens is capable of this range of deceleration ratio, and a three element zoom lens can accommodate a ratio of 15 while maintaining fairly good magnification characteristics.

When one considers the effect of requiring a deceleration ratio of 400 (this is the deceleration ratio needed to achieve 5-meV resolution using the same monochromator/analyzer configuration at 200–300 eV) it becomes apparent that this large deceleration ratio cannot be accomplished effectively in one stage. A single lens providing such a large deceleration ratio produces an image inside the lens field. The only suitable solution is a multistage lens system with one or more real images between the source and slit.

There are several possible approaches which can be adopted in extending the energy range of an existing EELS spectrometer. Three possibilities are: (1) redesign the entire lens system for the expanded energy range, (2) attempt to find suitable operating voltages which yield reasonable performance of the existing lens configuration, and (3) add some new lenses to the existing configuration. After some considerations based on general properties of electron optics and the characteristics of existing lens configurations of proven design, we decided that the third option presented the most attractive alternative. Option (2) can work in spectrometers having two or more lenses but, in our case, this option presented difficulty in terms of the new range of lens voltages required at high impact energies. This option would have required major changes in the existing control electronics.

Option (3) achieves a result which is nearly equivalent to the best result which would be expected from option (1) assuming the total number of lenses in each case is equal. Also, option (3) results in a design which maintains the original operating modes (lens voltages) by simply grounding the added lenses. The required lens voltages for the original lenses remained within the range available from the existing control unit, even when the optics are operated at 300-eV impact energy. This feature is a very convenient result of the design exercise. Essentially, we have shown that the addition of an extra lens can permit a factor of 15 increase in the energy range of EELS spectrometers while maintaining the energy resolution. No change in the voltage range of other spectrometer elements is required as long as the target can be operated at voltages different from ground potential.

III. NEW LENS CONFIGURATION

Figure 4 illustrates a cross-sectional view (in the scattering plane) of our old and new lens configurations. Our EELS spectrometer is a commercial tandem spectrometer (Leybold ELS-22) which is based on a pair of cylindrical analyzers (CDA-127°) and two element acceleration/deceleration lenses. The primary 127° sectors and lens systems are very similar to most of the single sector instruments[11] which have been constructed in various laboratories, and the lens system we have developed should function well on all of these instruments.

Most EELS spectrometers employ a circular electrostatic shield around the target to produce a field-free region near the scattering center. Electron acceleration and retardation are accomplished between lens elements which produce axial acceleration and focusing. Some spectrometers employ tube lenses (rotationally symmetric) and others employ lenses with rectangular apertures. The primary difference in these two lens configurations is that the rectangular lenses accommodate rectangular images slightly better, i.e., they tend to reduce chromatic aberrations along the major axis of a rectangular image. A three-element tube lens system with similar magnification properties should perform just as well as the rectangular lens system shown in Fig. 4.

In Fig. 4, existing components including lenses and the electrostatic shield are shown as solid lines; the new lens and shield are shown as dotted lines. The figure is drawn to scale, and the actual physical size is indicated by a 1-cm calibration mark. The original and new lens systems for the monochromator and analyzer sides of the spectrometer are identical; therefore, Fig. 4 illustrates only one side of the spectrometer optics. All three lenses of the monochromator and lenses L_1 and L_3 of the analyzer are split to provide beam steering capabilities. Lenses L_2 and L_3 are split parallel to the slit, L_1 is split perpendicular to the slit.

Our spectrometer had been operated for about 2 years before we added the new lenses, and we had established empirically, by tuning the instrument numerous times, a number of operating modes for resolutions ranging from 5 to 15 meV. We planned to use electron ray-tracing analysis to investigate the properties of the new lens system, and decided

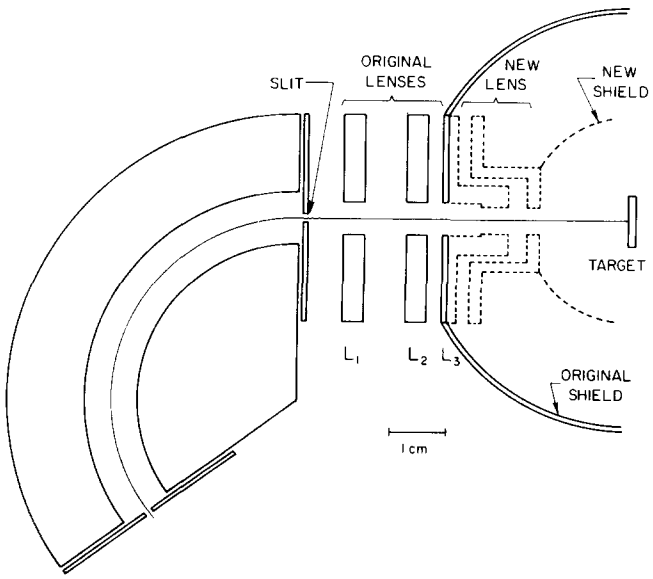

FIG. 4. Cross-sectional view of original (solid lines) and new lens system (dotted lines).

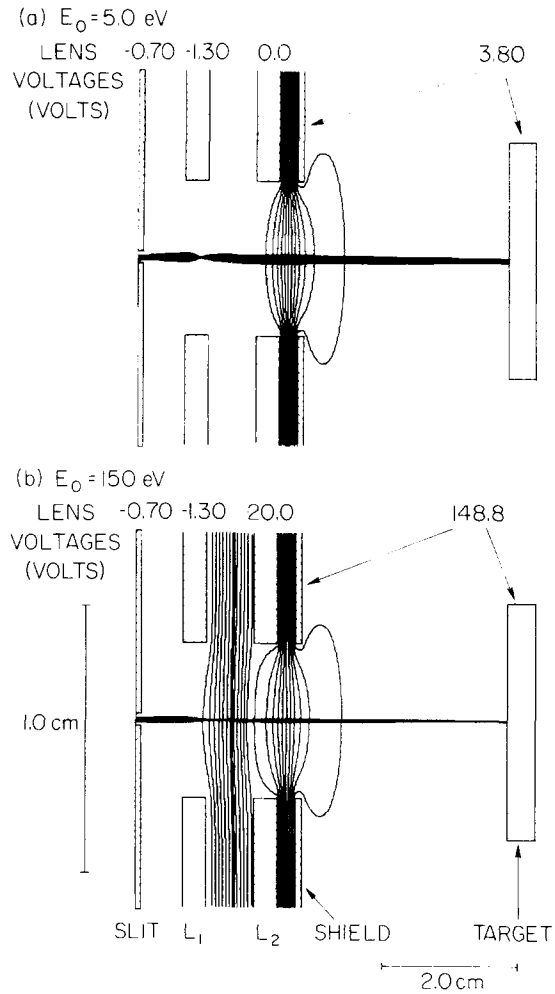

FIG. 5. Typical ray-tracing results for operating modes of the original lens system at two impact energies: (a) $E_i = 5$ eV; (b) $E_i = 150$ eV. Note difference between x and y scales.

to first apply these methods to the existing lens configuration with lens potentials specified by the voltages which had been established empirically.

The ray-tracing program we have used is a general-purpose program for computing fields and electron trajectories (W. B. Hermannsfeldt, S. L. A. C., Stanford University, 1973). We have used this program previously for developing an angle resolving photoelectron spectrometer,[14] and others have used it to evaluate input lens performance of a commercial ESCA spectrometer.[15] The program can accommodate either axial symmetric systems (i.e., a sequence of tube lenses), or systems having two-dimensional geometry (infinite extent in one dimension). We have found that ray-tracing results using either geometry can account for lens system behavior in applicable cases. We have conducted extensive ray-tracing studies of the tube lens system on our photoemission analyzer (using the axial symmetry program option) and of the original configuration of our EELS optics (using the two-dimensional program option). These studies have shown that ray-tracing results can be reconciled with empirical tests.[14]

Figure 5 displays ray-tracing results for two 10-meV resolution modes of the original lens configuration. Shown

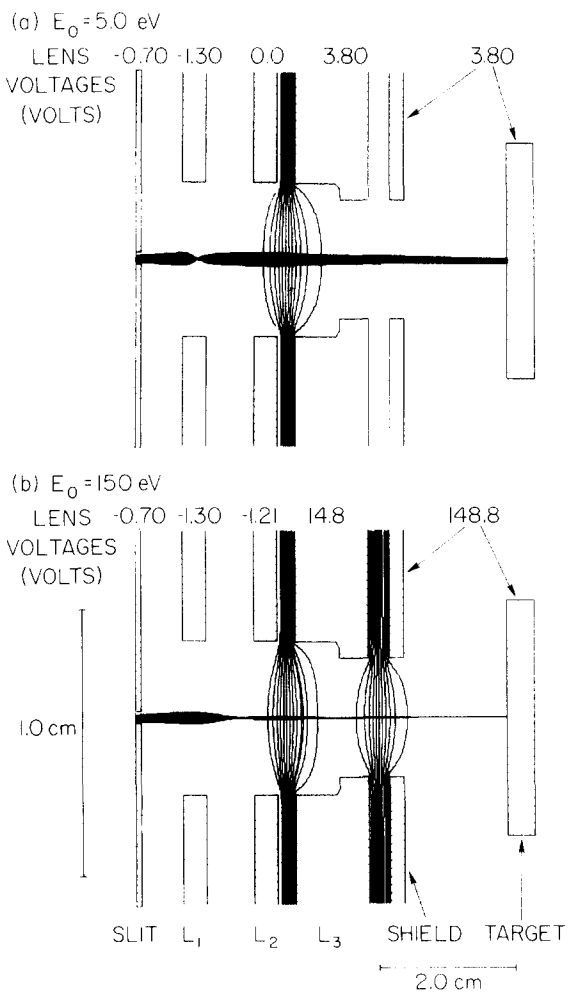

FIG. 6. Typical ray-tracing results for operating modes of the new lens system at two impact energies: (a) $E_i = 5$ eV; (b) $E_i = 150$ eV. Note difference between x and y scales.

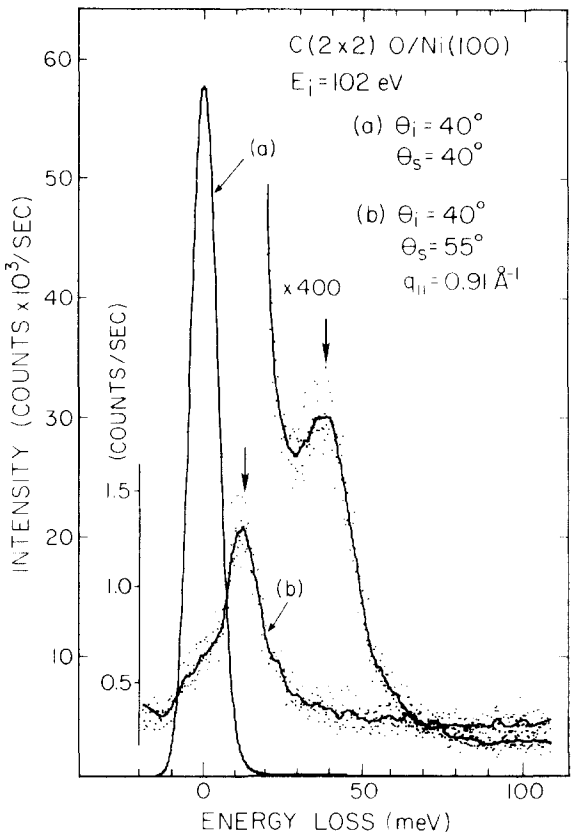

FIG. 7. EELS spectra for $c(2\times2)$O/Ni (100) at 102-eV impact energy. Curve (a) elastic peak and perpendicular oxygen vibrational loss peak observed in specular geometry. Curve (b) S_4 surface phonon peak observed in off-specular geometry. Note the elastic peak in curve (b) appears as only a shoulder.

in the figures are the monochromator exit slit, the two lenses, L_1 and L_2, the electrostatic shield, and the target. Figure 5(a) corresponds to 5-eV impact energy, and the equipotentials are shown for multiples of 8% of the acceleration voltage. Figure 5(b) corresponds to 150-eV impact energy, and in this case two sets of equipotentials are shown, each set corresponding to 8% of the acceleration voltage of each lens. Clearly, L_2 is the stronger lens. Referring to Fig. 5(b), one can observe that equipotential lines extend into the "field-free" region, and that L_2 affects the properties of L_1. Geometrical optics approximations and matrix optics methods would not provide accurate results in this particular instance.

Assumptions which were made in all of our EELS optics ray-tracing studies were: (1) the electrons emerged from the slit with kinetic energy equal to the pass energy (which is related to the slit potential), (2) the flux of electrons from the slit was uniform over the slit area and over an angular range which is limited by resolution considerations, and (3) the source area used when ray tracing electrons from the target to the analyzer was the area established by ray tracing from the monochromator to the target. The target area illuminated by the monochromator can also be estimated using the Helmholtz–Lagrange equation[14] based on assumptions (1) and (2), the accelerating potential, and the required angular resolution.

A number of ray-tracing studies of the original lens configuration (similar to the two cases shown in Fig. 5) estab-

lished that the modes which had been found empirically (by tuning the optics) correspond to beam profiles similar to those shown in the figure. The "correct" modes all seem to yield a narrow beam of electrons incident on the target, an image size comparable to the exit slit (near unity magnification), and a focal point near the plane of the lens nearest the slit. At low impact energies, as indicated in Fig. 5(a), most of the acceleration and deceleration of the beam occurs between the electrostatic shield and L_2.

Analogous ray-tracing studies of the new lens system based on voltages established by tuning the instrument were carried out to characterize operating modes at high impact energies. Figure 6 illustrates results for two modes corresponding to the same impact energies as for Fig. 5. Again, lens voltages which yield the best intensity at a given energy resolution yield a focal point near the plane of the lens nearest the slit. Notice that the 150-eV mode for the new lens system requires much lower L_1 and L_2 voltages compared with the corresponding voltages of the original lens configuration. Although not immediately apparent from Figs. 5 and 6, the 150-eV mode with three lenses has an angular spread one-fourth the value for the two lens system. This improves the $\Delta \mathbf{q}_{\parallel}$ resolution according to Eq. (5). Also, note that in the three lens configuration the potential lines do not penetrate the electrostatic shield as in the case of the two lens configuration.

When the new lens and target are connected to ground, the spectrometer operating modes are very nearly equivalent to the modes which were established prior to the lens modification, and the resolution and intensity of the instrument were not affected by the new lens system over the range where performance can be compared.

Figure 7 illustrates spectra for $c(2\times2)$O/Ni (100) obtained using the new lens system. Curves labeled (a) correspond to spectra taken at 102-eV impact energy in specular geometry ($\theta_i = \theta_s = 40°$). The loss peak at ~ 38 meV is produced by dipole scattering from the $O_\perp$ mode. Curve (b) corresponds again to the S_4 surface phonon of Ni (100) as shifted by the presence of $c(2\times2)$ oxygen. Note that the elastic peak intensity in this case ($\Delta\theta = 15°$) is reduced to a small shoulder to the left of the impact loss peak. There is no evidence of the $O_\perp$ mode in curve (b). These spectra clearly illustrate how impact scattering can be used to discriminate between dipole and impact loss structures in EELS spectra. The results of Fig. 7 are also plotted on the surface bands which appear as an inset in Fig. 2.

We have designed and tested a new lens system which permits high-resolution electron energy-loss spectroscopy measurements at high impact energies (several hundred eV). Our ray-tracing analysis of the original and new lens configurations has established the beam profiles and other beam parameters associated with one of the more popular EELS spectrometer configurations. The ray-tracing studies have also shown that operating modes established empirically by tuning EELS spectrometers (having real slits) for maximum intensity correspond to desirable beam properties including a small image at the target, small angular divergence, and efficient beam focusing at the monochromator entrance slit. Application of EELS at high impact energies has been demonstrated by mapping the surface phonon bands of $c(2\times2)$O/Ni (100) along the $\bar{\Delta}$ line of the surface Brillouin zone.

ACKNOWLEDGMENT

This work was sponsored by the Air Force Office of Scientific Research under Grant No. AFOSR-83-0131.

[1]R. L. Strong, B. Firey, F. W. deWette, and J. L. Erskine, Phys. Rev. B **25**, 5547 (1982).
[2]R. L. Strong and J. L. Erskine (to be published).
[3]J. M. Szeftel, S. Lehwald, H. Ibach, T. S. Rahman, J. E. Black, and D. L. Mills, Phys. Rev. Lett. **51**, 268 (1983).
[4]S. Lehwald, J. M. Szeftel, H. Ibach, T. S. Rahman, and D. L. Mills, Phys. Rev. Lett. **50**, 518 (1983).
[5]S. Y. Tong, C. H. Li, and D. L. Mills, Phys. Rev. Lett. **44**, 407 (1980).
[6]W. Ho, R. F. Willis, and E. W. Plummer, Phys. Rev. B **21**, 4202 (1980).
[7]E. Evans and D. L. Mills, Phys. Rev. B **5**, 4126 (1971).
[8]G. C. Aers, T. B. Grimley, J. B. Pendry, and K. L. Sebastian, J. Phys. C **14**, 3995 (1981).
[9]R. E. Allen, G. P. Alldredge, and F. W. deWette, Phys. Rev. B **4**, 1661 (1971).
[10]J. E. Demuth, K. Christman, and P. N. Sanda, Chem. Phys. Lett. **76**, 201 (1980); N. R. Avery, Appl. Surf. Sci. **13**, 171 (1982); G. E. Thomas and W. H. Weinberg, Rev. Sci. Instrum. **50**, 497 (1979).
[11]L. L. Kesmodel, J. Vac. Sci. Technol. A **1**, 1456 (1983); M. Nishijima, S. Masuda, H. Kobayashi, and M. Onchi, Rev. Sci. Instrum. **53**, 790 (1982); B. A. Sexton, J. Vac. Sci. Technol. **16**, 1033 (1979); H. Ibach and D. Bruchmann, Phys. Rev. Lett. **41**, 958 (1978); H. Ehrhardt, L. Langhans, F. Linder, and H. S. Taylor, Phys. Rev. **73**, 222 (1968).
[12]S. Andersson and M. Persson, Phys. Rev. B **24**, 3659 (1981).
[13]D. Roy and J. D. Carette, in *Electron Spectroscopy for Surface Analysis*, edited by H. Ibach (Springer, Berlin, 1977).
[14]G. K. Ovrebo and J. L. Erskine, J. Electron Spectrosc. Relat. Phenom. **24**, 189 (1981); H. A. Stevens, A. W. Donoho, A. M. Turner, and J. L. Erskine, *ibid.* **32**, 327 (1983).
[15]P. J. Orders, M. Sagurton, and C. S. Fadley, J. Electron Spectrosc. Relat. Phenom. (in press).